20

Desrochers, André, Denis Lavoie, Patricia Brennan-Alpert, and Guoxiang Chi, 2012, Regional stratigraphic, depositional, and diagenetic patterns of the interior of St. Lawrence platform: The Lower Ordovician Romaine Formation, western Anticosti Basin, Quebec, *in* J. R. Derby, R. D. Fritz, S. A. Longacre, W. A. Morgan, and C. A. Sternbach, eds., The great American carbonate bank: The geology and economic resources of the Cambrian–Ordovician Sauk megasequence of Laurentia: AAPG Memoir 98, p. 525–543.

Regional Stratigraphic, Depositional, and Diagenetic Patterns of the Interior of St. Lawrence Platform: The Lower Ordovician Romaine Formation, Western Anticosti Basin, Quebec

André Desrochers and Patricia Brennan-Alpert

Ottawa-Carleton Geoscience Centre, Department of Earth Sciences, University of Ottawa, Ottawa, Ontario, Canada

Denis Lavoie

Geological Survey of Canada, Commission Géologique du Canada Quebec, Natural Resources Canada, Quebec, Quebec, Canada

Guoxiang Chi

Department of Geology, University of Regina, Regina, Saskatchewan, Canada

ABSTRACT

Lower Ordovician to lower Middle Ordovician (upper Ibexian to lower Whiterockian; upper Sauk III supersequence) subtidal to peritidal carbonates of the Romaine Formation in the western Anticosti Basin record the evolution during the early Paleozoic of the low-latitude passive margin of eastern North America. A regional paleokarst unconformity, the super-Romaine unconformity corresponding to the North American Sauk-Tippecanoe megasequence boundary developed on top of the Romaine carbonates during the early Middle Ordovician. The regional distribution of the passive-margin carbonates below the unconformity, however, suggests that significant foreland basin tectonic activity influenced the facies patterns in the uppermost Romaine Formation before the final demise of the Lower Ordovician great American carbonate bank, leading to its eventual subaerial exposure and erosion.

The Romaine Formation is mostly composed of peritidal and open-shelf carbonate rocks similar to those in age-equivalent El Paso, Ellenburger, Arbuckle, Knox, Beekmantown, and St. George Groups found along the present southern and eastern flanks of the North American craton. Flooding of the Precambrian basement for the first time in the area allowed deposition of a deepening to shallowing carbonate succession in the late Ibexian. A narrow coastal belt of peritidal carbonates onlapped onto the basement with time, but the Romaine platform was

DOI:10.1306/13331505M983504

mostly covered by open-marine subtidal carbonate deposits. The latter, as sea level receded and offlap began, gave way to peritidal deposition in the latest Ibexian. However, a succession of lower Whiterockian subtidal limestone found locally in the offlapping carbonates indicates that open subtidal conditions resumed briefly before the super-Romaine unconformity formed. This Romaine stratigraphy suggests that two large-scale, third-order, transgressive-regressive sequences are present and can be correlated basinward into the subsurface beneath the northern part of Anticosti Island.

Petrographic and geochemical interpretations combined with other geologic and geophysical data provide evidence that the Lower Ordovician carbonates were hydrothermally altered at a regional scale to form porous, structurally controlled dolostone reservoirs. These structurally controlled hydrothermal dolomite reservoirs in the Romaine Formation provide a local but significant trapping mechanism for migrating hydrocarbons along the relatively undeformed, southwesterly dipping homoclinal succession. Their signature has been recognized along several seismic lines and has served as an exploration guide in the recent round of exploration on Anticosti Island.

INTRODUCTION

During the early Paleozoic, extensive epeiric carbonate platforms developed across the North American craton (also termed the great American carbonate bank by R. N. Ginsburg) when sea level stand was relatively high. In the Quebec reentrant and adjacent St. Lawrence promontory of the northern Appalachians (Thomas, 1977; James et al., 1989; Lavoie, 2008), these epeiric carbonates recorded the evolution during the early Paleozoic of the low-latitude passive margin of eastern North America before the onset of the Taconic orogeny. Shallow-water carbonates of Cambrian–Ordovician age that originally lay along the outer edge near the ancient continental margin are now exposed along the extensive relatively undeformed outcrop belts in western Newfoundland (Knight and James, 1987; Lavoie et al., 2003). Parts of this once extensive shelf, however, are now exposed in the Quebec reentrant and are collectively known as the St. Lawrence platform (Sanford, 1993). The St. Lawrence platform has been divided into the occidental (Michigan and Alleghany Basins), central (Ottawa embayment and Quebec Basin), and oriental (Anticosti Basin) segments (Sanford, 1993). In eastern Quebec, at the major transform fault that links the reentrant and the promontory, most of the platform interior lies beneath the Gulf of St. Lawrence except for small but important outcrops in the Mingan Islands of eastern Quebec located 300 km (186 mi) west of Newfoundland (Desrochers and James, 1988) (Figure 1). The Lower Ordovician carbonate facies of the Romaine Formation on the Mingan Islands are typical of the inner cratonic dolomite facies widely observed across North America and were pervasively dolomitized early in their history. Despite their pervasive dolomitization, these carbonates display well-preserved megascopic details and are superbly exposed along extensive coastal exposures in the Mingan Islands. The stratigraphy of these rocks in the Mingan Islands has been published (Desrochers and James, 1988), but their sedimentology has never been documented in a systematic fashion.

Hydrocarbon exploration on Anticosti Island (a large island ~8000 km^2 [~3090 mi^2] in size located south of the Mingan Islands; Figure 1) in the past 40 yr resulted in the acquisition of more than 800 km (>500 mi) of seismic data and the drilling of 16 exploration wells (Lynch, 2001; Lavoie et al., 2005). Some of these wells encountered porous reservoir units in both Lower and Middle Ordovician carbonates. The Anticosti seismic and drilling data provide invaluable subsurface information on the more outer cratonic mixed dolomite-limestone facies, equivalent to those present in the Mingan Islands. During recent years, core, seismic, petrographic, and geochemical studies (Brennan-Alpert, 2001; Chi and Lavoie, 2001; Lynch and Trollope, 2001) all independently suggested hydrothermal alteration of the Lower Ordovician carbonates of the St. Lawrence platform on Anticosti Island. Although Ellenberger-type paleokarst plays are present, the regional presence of hydrothermally enhanced reservoirs at the base of a thick carbonate succession is a key element in the ongoing exploration efforts on the island (Lavoie et al., 2005).

The main objective of this chapter was first to integrate results from our own independent stratigraphic, sedimentologic, and diagenetic studies undertaken during the last decade and to present a coherent picture of platform evolution across the western Anticosti Basin during the Early Ordovician. In addition, we want to take our regional analysis a step further using a sequence-stratigraphic approach to document the shelf

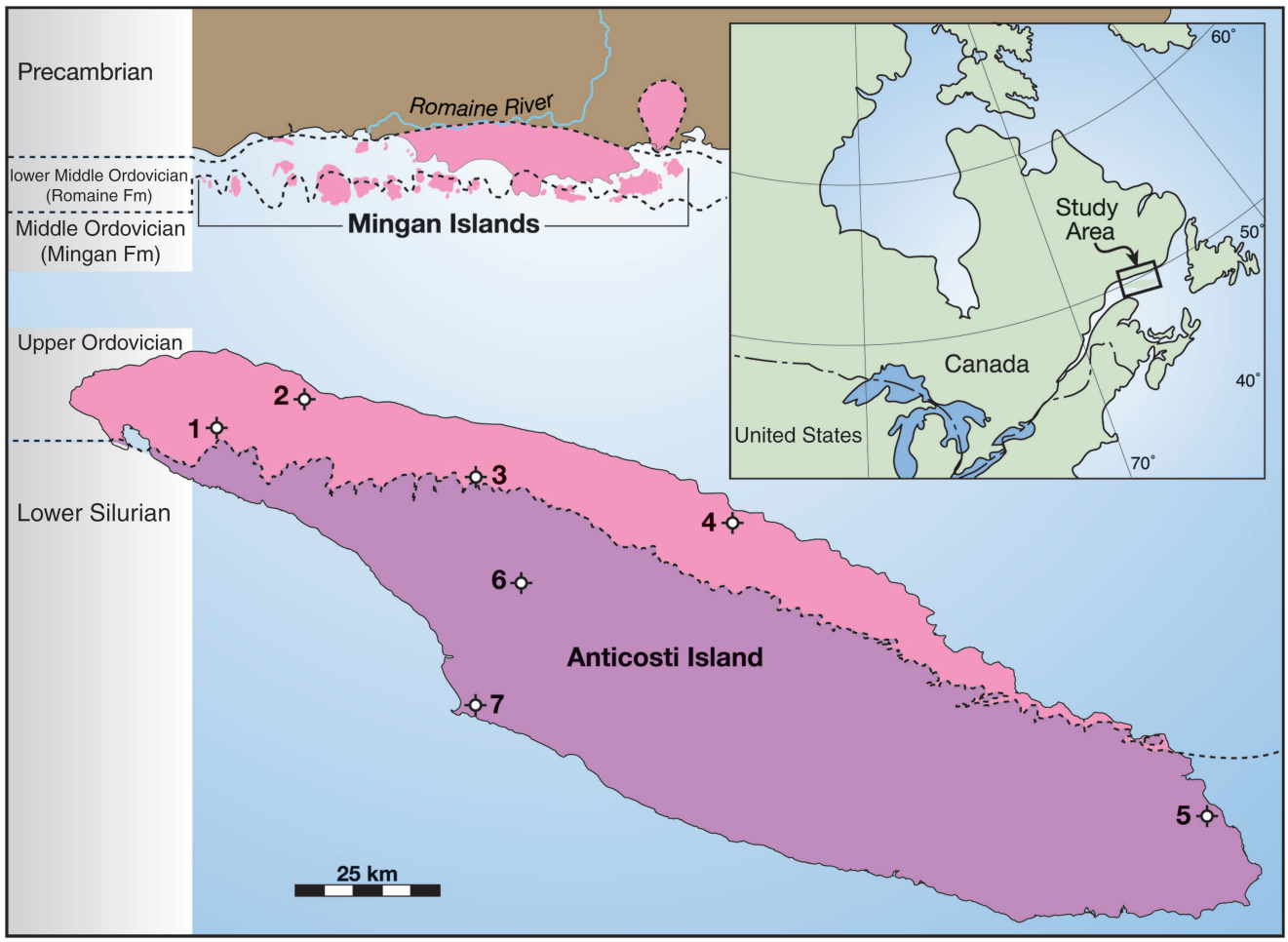

Figure 1. An index map showing the location of the study area in eastern North America and a geologic map showing Lower Ordovician to Lower Silurian strata exposed along the Mingan Islands and on Anticosti Island (modified from Desrochers, 1985; Desrochers and Gauthier, 2009). Subsurface data used in this study are from the following drill cores on Anticosti Island: (1) Lowlands-Gamache 1 Princeton Lake, (2) Lowlands-Gamache 1 Highcliff, (3) Lowlands-Gamache 1 Oil River, (4) Lowlands-Gamache 1 Carleton Point, (5) Scurry Rainbow 1 Sandtop, (6) New Associated Consolidated Paper 1 Anticosti, (7) ARCO 1 Anticosti. 25 km (15.5 mi).

architecture in which both large- and small-scale shallow-water carbonate cycles are present. Finally, some regional diagenetic features and exploration play types will be outlined.

WESTERN ANTICOSTI BASIN

The Anticosti Basin represents the eastern segment of the St. Lawrence platform and is separated from the latter's central segment (Quebec Basin) by the Saguenay arch (Sanford, 1993). The basin is bounded on the north by Precambrian terranes of the Canadian shield (Grenville structural province) and to the southeast and southwest (western Newfoundland and Gaspe, respectively) by thrusted terranes of the Appalachian orogeny (Figures 1, 2). The Anticosti Basin is divided by the south-trending Beauge arch (Figure 2) into a western part that preserves Lower Ordovician to Upper(?) Silurian strata probably in excess of 8000 m (26,250 ft) in thickness and an eastern part that comprises up to 6000 m (19,685 ft) of Lower Cambrian to Devonian (Emsian) strata offshore of western Newfoundland (Sanford, 1993). This study focuses on the western segment of the Anticosti Basin.

The western Anticosti Basin is mostly concealed beneath the waters of the northern part of the Gulf of St. Lawrence and its adjacent estuary (Mossop et al., 2004) but rises to the surface to form bedrock along the Mingan Islands, the adjacent mainland, and on Anticosti Island (Desrochers and James, 1988; Sanford, 1993; Long, 2007). There, preserved Lower Ordovician to Lower Silurian strata (Figures 1, 2) recorded a transition from a passive-margin setting to a tectonically

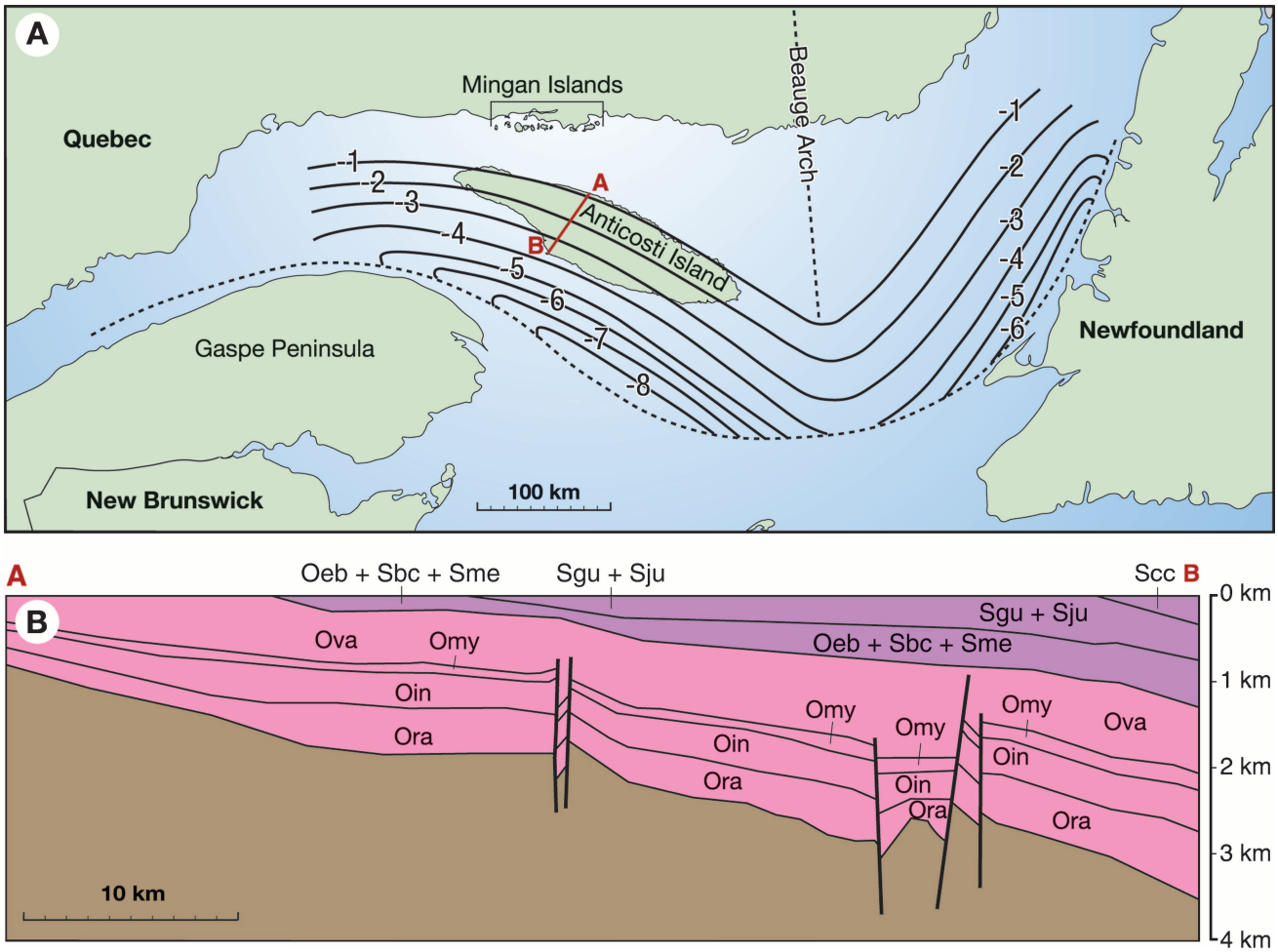

Figure 2. (A) Depth to basement below sea level in the Anticosti Basin (contours in kilometers) north of the probable northern limit of Acadian deformation (dashed line). Note the location of the Beauge arch separating the Anticosti Basin into western and eastern parts (modified from Sanford, 1993); (B) AB structural cross section showing Lower Ordovician to Lower Silurian strata present below Anticosti Island based on seismic and core correlations (modified from Roksandic and Granger, 1981; Brennan-Alpert, 2001; Castonguay et al., 2005). Ora = Romaine; Oin = Mingan; Omy = Macasty; Ova = Vaureal; Oeb = Ellis Bay; Sbc = Becscie; Sme = Merrimack; Sgu = Gun River; Sju = Jupiter; Scc = Chicotte. 10 km (6.2 mi).

active foreland basin to a post-Taconic successor basin. The foreland basin was related to the emplacement of Taconic thrust sheets farther to the south over the northern part of the Gaspe Peninsula and over parts of the St. Lawrence Estuary and Gulf (Pinet et al., 2008). The subsequent post-Taconic successor basin was affected by minor Acadian tectonic stresses (Bordet et al., 2010).

The passive-margin record consists of Lower Ordovician to lower Middle Ordovician subtidal to peritidal carbonates of the upper Ibexian to lower Whiterockian Romaine Formation, which is part of the upper Sauk III supersequence and unconformably overlies the Grenvillian metamorphic basement (Figure 3). The Romaine strata of the Mingan Islands area are up to 75 m (250 ft) thick and dip southwestward in the offshore beneath younger Ordovician and Silurian beds to reach a thickness of 400 and 800 m (1310 and 2625 ft) beneath the north-central part and south-central part of Anticosti Island, respectively (Castonguay et al., 2005) (Figures 2, 4). In the Mingan Islands, the Romaine Formation yields diagnostic fossils (e.g., conodont, graptolites, brachiopods, and trilobites) equivalent to the faunal unit D in the basal siliciclastic beds (Figure 3) to faunal unit E as little as 15 m (50 ft) above the base of the formation and to faunal unit 1-2 in some fossiliferous limestone beds present at the top of the formation in the western part of the Mingan Islands (Desrochers and James, 1988). The regional distribution of these passive-margin carbonates was, however, modified by faulting, uplift, and erosion during the initial stages of the Taconic orogeny (Lynch, 2001; Bordet et al., 2010). Stratigraphic thinning and complete erosion of the Romaine carbonates

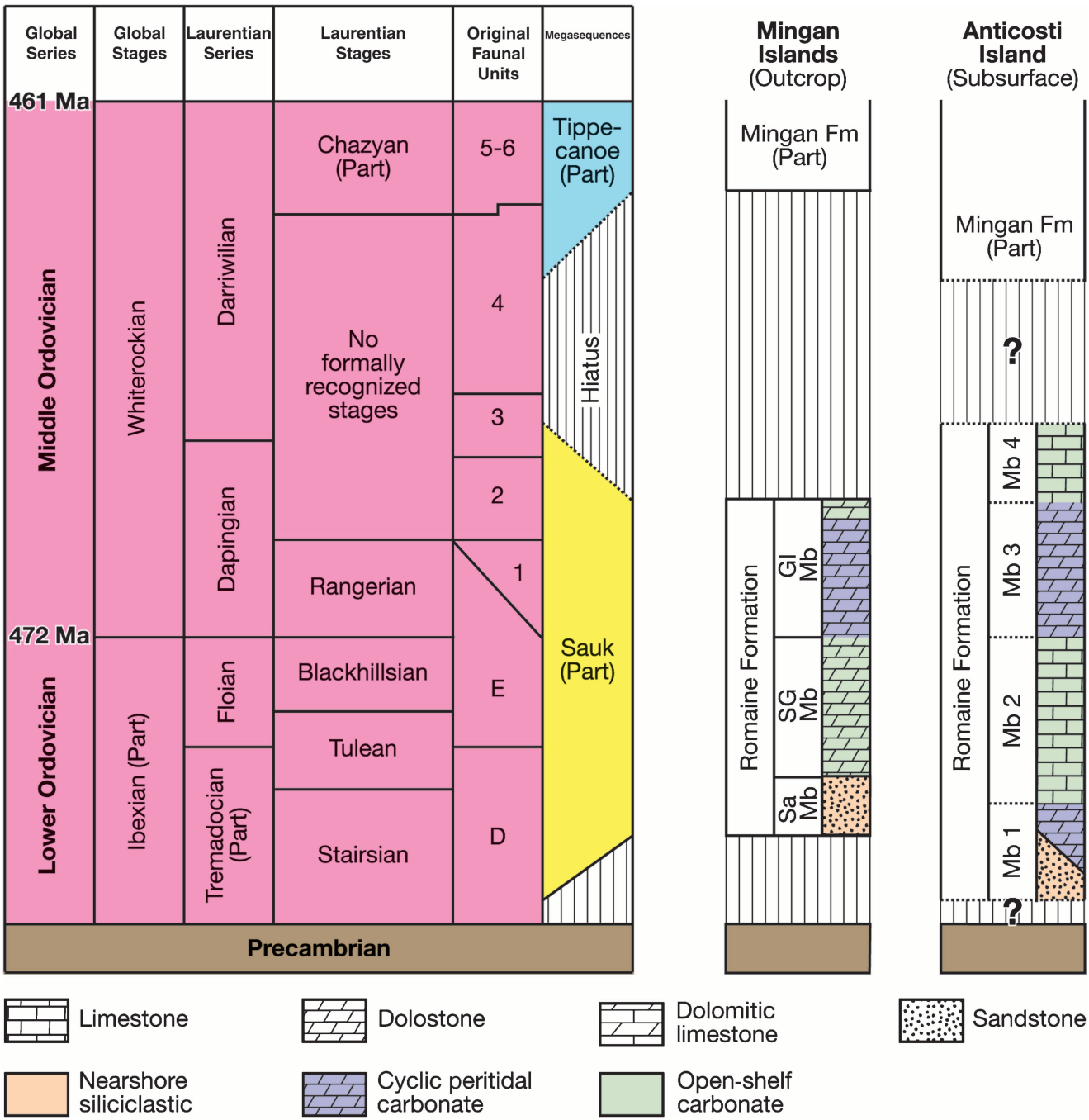

Figure 3. The stratigraphic position of the Romaine Formation in outcrop (Mingan Islands) and subsurface (Anticosti Island) against global and Laurentian Ordovician series and stages and Laurentian original faunal units and megasequences. Members (Mb) of the Romaine Formation are formal units in the Mingan Islands. Sa Mb = Sauvage Member; SG Mb = St. Genevieve Member; GI Mb = Grande Ile Member and informal units in the subsurface below Anticosti Island (Mb 1–4).

toward the Beauge arch (Figure 4) suggest that the arch was a positive and likely active feature during and following their depositional period (Desrochers, 1985; Sanford, 1993; Lynch, 2001). The Romaine Formation in the western Anticosti Basin is capped by a lower Middle Ordovician unconformity (termed here the super-Romaine unconformity) that corresponds to the Sauk-Tippecanoe sequence boundary of Sloss (1963). The super-Romaine unconformity is overlain by middle to upper Whiterockian limestones of the Mingan

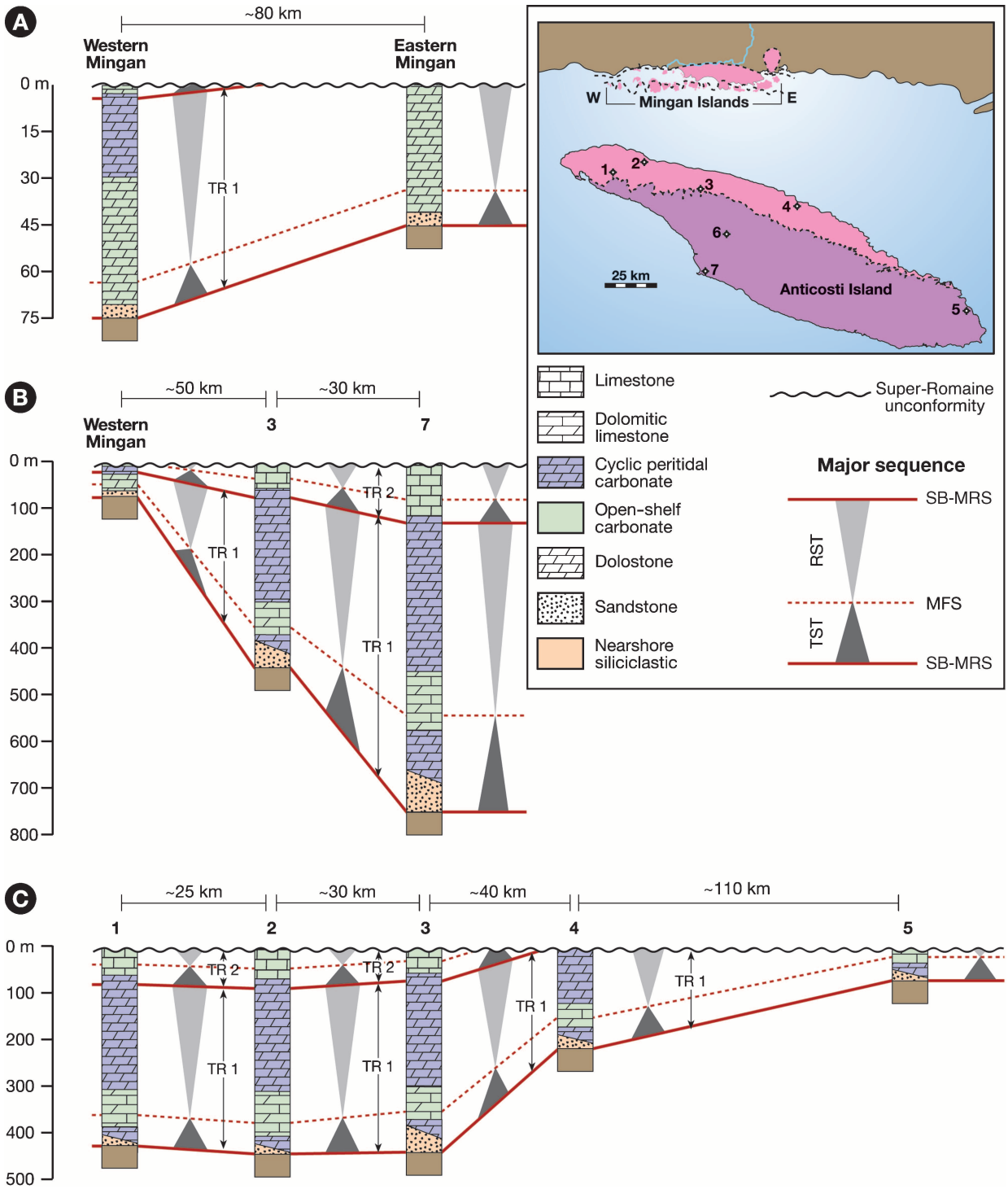

Figure 4. (A) Generalized stratigraphic and lithologic columns showing the distribution of the major Romaine transgressive-regressive (TR) sequences in the Mingan Islands (modified from Desrochers, 1985). (B) Generalized stratigraphic and lithologic columns showing the distribution of the major Romaine TR sequences along dip from the western Mingan Islands to the south-central part of Anticosti Island (modified from Brennan-Alpert, 2001). (C) Generalized stratigraphic and lithologic columns showing the distribution of the major Romaine TR sequences in subsurface along strike in the northern part of Anticosti Island (modified from Brennan-Alpert, 2001). Note the progressive thinning of the Romaine Formation toward the Beauge arch by erosion at the super-Romaine unconformity in A and C. See Figure 1 for the names of the drill cores. TST = transgressive systems tract; RST = regressive systems tract; SB-MRS = sequence boundary-maximum regressive tract; MFS = maximum flooding surface. 100 m (328 ft); 10 km (6.2 mi).

Formation in which diagnostic fossils equivalent to the Chazyan faunal unit 5–6 are present (Desrochers and James, 1988) (Figure 3). The super-Romaine unconformity is a well-developed karst unconformity in the Mingan Islands that can be traced seaward to a disconformity beneath Anticosti Island. On the Mingan Islands, the paleokarst unconformity displays various surface (e.g., karren, collapse dolines) and subsurface solution features as much as 30 m (100 ft) below the unconformity (e.g., small caves filled with collapse breccias). The super-Romaine unconformity was clearly fashioned by early Taconic orogenic events parallel with eustatic events (Desrochers and James, 1988). Similar unconformities that span the length of the Appalachian system (St. George, Beekmantown, intra-Philipsburg, and Knox unconformities) are interpreted to result from the more or less pronounced subaerial exposure of the Lower Ordovician platform carbonates in response to the rapid westward-sweeping migration of a Taconic peripheral lithospheric bulge (Knight et al., 1991; Lavoie, 1994; Salad Hersi and Dix, 2006; Salad Hersi et al., 2007). Moreover, recent detailed work on the Romaine (Lavoie et al., 2005; Lavoie and Chi, 2010) and adjacent coeval platform carbonates in the Quebec reentrant (Dix and Al Rodhan, 2006; Salad Hersi et al., 2007; Dix, 2012) suggests that the inception of significant foreland basin tectonic activity (and hence some controls on depositional facies patterns) started before subaerial exposure and final demise of the Lower Ordovician great American carbonate bank.

SEDIMENTOLOGY OF THE ROMAINE FORMATION

Eight distinct lithofacies are present in the Romaine Formation in both outcrops and subsurface (for a summary, see Table 1, Figure 5). At the regional scale, dolomitization of the Romaine Formation decreases basinward (southwestward); although peritidal facies are pervasively dolomitized, subtidal facies are either only partly dolomitized or undolomitized, as seen in the Anticosti cores.

In outcrop, the Romaine lithofacies are grouped into three facies assemblages (Figure 4A): (1) a basal nearshore siliciclastic facies assemblage (lithofacies A); (2) a middle assemblage of open-shelf carbonates (lithofacies B and C); and (3) an upper assemblage of cyclic peritidal carbonates (lithofacies D, E, F, G, and H). The lower assemblage (Sauvage Member in Figure 3) consists of an arkosic sandstone unit (lithofacies A), which directly overlies Precambrian basement. The sandstone unit reaches 3 m (10 ft) in thickness. The lower to middle assemblage contact is not exposed. The middle assemblage (St. Genevieve Member in Figure 3) is well exposed in coastal exposures along the north shore of the Gulf of St. Lawrence and along the inner Mingan Islands, where it ranges from 40 to 45 m (130–150 ft) in thickness (Figures 1, 4A). The lower 25 to 30 m (80–100 ft) is mainly composed of thin- to medium-bedded burrow-mottled dolostone (lithofacies B; Figure 5F). Thrombolite mounds and associated lithologies (lithofacies C) form most of the upper part of the middle assemblage (15–20 m [50–66 ft]). The thrombolite mounds occur either as small submeter isolated buildups (Figure 5H) or as closely spaced buildups forming larger reefal complexes (Figure 5G) stratigraphically superimposed into massive units (up to 6 m [20 ft] thick). The upper assemblage (Grande Ile Member in Figure 3), exposed mainly along the coastal exposures on several of the large outer Mingan Islands in the central and western parts of the study area, is approximately 30 m (100 ft) thick and is characterized by a cyclic repetition of peritidal lithofacies on a meter scale (Figures 1, 4A). Two distinct idealized meter-scale cycles are recognized but only differ in their basal lithofacies. The basal lithofacies consists of either burrowed dolomicrite (lithofacies E; Figure 5D) or ooid dolostone (lithofacies D; Figure 5E). They grade up into stromatolitic dolomicrite (lithofacies F; Figure 5C) and ripple-laminated dolomicrite (lithofacies G; Figure 5B). The cycles are commonly capped by dololaminite (lithofacies H; Figure 5A). The cycles have sharp bases, sometimes overlain by intraformational conglomerate. The lithofacies contacts, however, are gradual within each cycle. Individual peritidal cycles range from 2 to 4 m (6.6–13 ft) in thickness. In the western Mingan Islands, these meter-scale cycles, if not eroded by the super-Romaine paleokarst unconformity, have been successfully traced over 20 km (12.4 mi) from several closely spaced sections, with only minor changes in their thickness or in their internal lithofacies organization.

In the subsurface beneath Anticosti Island, the vertical and lateral distribution of the Romaine facies assemblages is illustrated by cross sections oriented along both the strike and dip (Figure 4B, C). Above a basal nearshore siliciclastic unit, four facies assemblages are present from base to top: (1) a lower cyclic peritidal facies assemblage (informal member 1 in Figure 3) that is not well developed in the Mingan Islands, (2) a lower subtidal facies assemblage (informal member 2 in Figure 3) similar to the middle assemblage exposed in the Mingan Islands, (3) an upper cyclic peritidal facies assemblage (informal member 3 in Figure 3) similar to the upper assemblage exposed in the Mingan Islands, and (4) an upper subtidal facies assemblage (informal member 4 in Figure 3) present also in the Mingan Islands but only in the youngest strata in the western

Table 1. Summary of the facies assemblages in the Romaine Formation.*

Lithofacies	Description	Interpretation	Distribution
Nearshore Siliciclastic Facies Assemblage			
Feldspathic sandstone (A)	20–30% feldspar; texturally mature; cross-stratified; restricted marine fauna; common *Skolithos*	Nearshore sand belt	Basal transgressive assemblage in outcrops; present but poorly recovered in cores
Open-shelf Carbonate Facies Assemblage			
Burrow-mottled dolosparite (B)	Intensely bioturbated (mostly *Palaeophycus*); dolomudstone or wackestone interbedded with some coarser grained tempestites; open-marine fauna including graptolites	Open shelf below fair-weather wave base	Lower part of the Romaine (St. Genevieve Member) in outcrops; dominant lithofacies in subtidal intervals of the Anticosti cores
Thrombolite mounds and complexes (C)	Isolated to closely spaced mounds, 0.5–3 m (1.6–10 ft) high and 0.5 to 20 m (1.6–66 ft) wide; thrombolites with typical mesoclotted fabric; associated archeoscyphid sponges; intraclastic-rich channels in flanks	Onshelf microbial or sponge patch reefs	Lower part of the Romaine in outcrops (St. Genevieve Member) and in cores (member 2)
Peritidal Carbonate Facies Assemblage			
Laminated dolomicrite or dololaminite (D)	Parallel- and wavy laminated; desiccation cracks; tepee structures; flat-pebble conglomerates; evaporite pseudomorphs	Supratidal sabkha	Capping facies in meter-scale peritidal cycles; present in both cores and outcrops
Ripple-laminated dolomicrite (E)	Parallel- to wavy laminated with flaser and lenticular bedding; rare desiccation cracks	Intertidal mixed mud and sandflats	Middle part in meter-scale peritidal cycles; present in both cores and outcrops
Stromatolite beds and mounds (F)	Laterally linked hemispheroid stromatolite beds to meter-scale mounds with digitate columns; desiccation cracks; dolomicrites	Intertidal to shallow subtidal microbial mats	Middle part in meter-scale peritidal cycles; present in both cores and outcrops
Burrow-mottled dolomicrite (G)	Moderate to intense bioturbation; restricted stenohaline fauna, peloid-rich dolomudstone or wackestone	Semirestricted lagoon	Basal part in some meter-scale peritidal cycles; present in both cores and outcrops
Ooid dolograinstone (H)	Massive to cross-laminated unit; well-sorted medium sand-size ooids with both radial and concentric cortices	Nearshore oolitic sand belts	Basal part in some meter-scale peritidal cycles; present in both cores and outcrops

*Modified from Desrochers (1985) and Brennan-Alpert (2001).

part. The present lateral continuity of these facies assemblages is clearly related to the super-Romaine unconformity, truncating progressively older strata in a northeastern direction (Figure 4).

The Romaine Formation is mostly composed of peritidal and open-shelf carbonates similar to those in the age-equivalent El Paso, Ellenburger, Arbuckle, Knox, Beekmantown, and St. George Groups, which represent the remnants of a Cambrian–Ordovician great American carbonate bank stretching along the present southern and eastern flanks of the North American craton (Wilson et al., 1992). Of particular interest, the Romaine Formation strata (i.e., St. Genevieve and Grande Ile Members) can be correlated over 500 km (310 mi) across the Gulf of St. Lawrence with equivalent units (i.e., Catoche and Aguathuna Formations of the upper St. George Group, respectively) in western Newfoundland (Desrochers, 1985). After initial flooding of the Precambrian basement and localized peritidal deposition in the late Ibexian, the sedimentation regime across the Romaine platform changed through time from dominantly open subtidal to peritidal deposition. Localized strandline sands (Mingan Islands) and peritidal deposition (subsurface, Anticosti Island) was established on the Romaine platform after marine flooding of Precambrian basement in this area for the first time. The basal strandline sandstone and peritidal carbonate flats were onlapped and overstepped by subtidal carbonates as sea level continued to rise across the Quebec margin. These carbonates were, in time, succeeded by peritidal carbonates in the latest Ibexian as sea level rise gradually slowed, the shoreline receded, and tidal flats prograded out across the shelf. During the subtidal phase, extensive thrombolite patch reefs developed on the platform with possibly stranded tidal flats located north of the Mingan Islands. These reef complexes were located in the platform interior at least several hundred kilometers away from the platform margin, which in western Newfoundland, at least, is known to have been dominated by different buildups composed of calcified algae (James, 1981; Pohler et al., 1987). As time passed, cyclic peritidal sedimentation prevailed across the platform (i.e., Grande Ile Member of the Mingan Islands and its subsurface equivalents). Inner-shelf lithofacies (dololaminites, stromatolites) formed an extensive coastal tidal flat close to the cratonic margin, whereas typical cyclic peritidal carbonate sedimentation including ripple-laminated dolomicrites representing mixed sand and mud intertidal flat sediments (Demicco and Hardie, 1994) developed in a more outboard marine setting of island tidal flats (Pratt and James, 1986). Finally, open subtidal conditions resumed briefly during the early Whiterockian; the resulting carbonates form the topmost interval of the preserved Romaine section preserved below the super-Romaine unconformity. The regional distribution of these subtidal carbonates suggests local tectonic control allowed renewed flooding only to be interrupted by sea level fall and disconformity formation. In a similar way, the Carillon Formation with its regionally variable thickness forms the topmost unit of the Lower Ordovician carbonate platforms in southern Quebec and eastern Ontario (Salad Hersi et al., 2003, 2007; Dix and Al Rodhan, 2006). There, the first pulses of foreland basin tectonism in front of the migrating lithospheric bulge likely controlled the sedimentation patterns and facies of this formation.

SEQUENCE STRATIGRAPHY OF THE ROMAINE FORMATION

The sequence-stratigraphic framework of the Romaine Formation in the western Anticosti Basin is illustrated in Figure 4. Two large-scale, third-order, transgressive-regressive (TR) sequences are present and correlate basinward from the Mingan Islands to the subsurface beneath the northern part of Anticosti Island. Older Lower Ordovician and possibly Middle and Upper Cambrian third-order sequences have been hypothesized beneath the west-central and southern shore of Anticosti Island (Sanford, 1998; Lynch, 2001). However, they are not seen in any of the deep drill holes beneath the island or recent offshore seismic profiles in the Gulf of St. Lawrence. The first TR sequence (TR-1) is bounded at the base by the Precambrian basement and at the top by a disconformity separating upper Ibexian from overlying Whiterockian strata in the Mingan Islands. The upper sequence boundary can be traced basinward in the subsurface into a zone, instead of a distinct surface, composed of meter-scale peritidal cycles dominated by evaporitic intertidal-supratidal facies. Although progressively truncated updip by the super-Romaine unconformity, TR-1 is about 60 m (200 ft) thick in the western Mingan Islands and thickens to 320 m (1050 ft) in the northwestern part of the Anticosti Island, a nearly fivefold increase across less than 100 km (<62 mi) (Figure 4B). The transgressive systems tract of sequence 1 is composed of the basal nearshore siliciclastics, overlain by onlapping cyclic peritidal and open-marine shelf carbonates. The maximum flooding surface or zone is hidden in the lower part of the subtidal carbonate of the St. Genevieve Member, which represents a period when open-marine conditions existed across the entire St. Lawrence Platform as described later in this chapter. The regressive systems tract (RST) above the maximum flooding surface or zone comprises

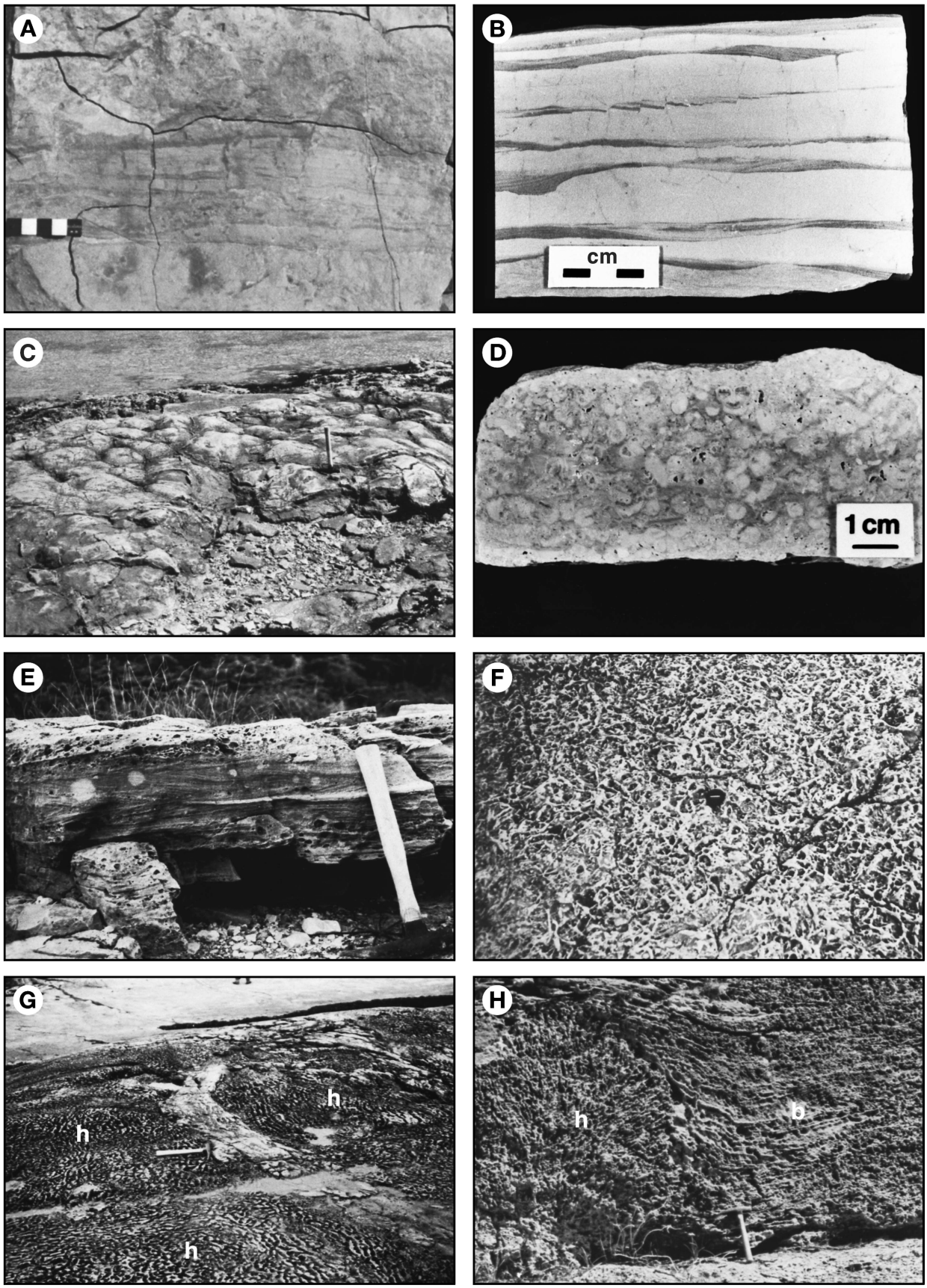
A
B
cm
C
D
1 cm
E
F
G
h
h
h
H
h
b

progressively shallower, storm-influenced, subtidal carbonates capped by thrombolite or sponge reefal limestones (upper St. Genevieve Member) that are overlain by meter-scale peritidal carbonate cycles (Grande Ile Member). The TR-1 with peritidal deposits defining its base and upper parts is remarkably similar to a coeval third-order sequence present in the upper St. George Group of western Newfoundland (i.e., upper Boat Harbour, Catoche, and Aguathuna Formations; Knight and James, 1987; James et al., 1989). This suggests a strong eustatic control on the development of an extensive cratonic platform on the St. Lawrence Promontory during the late Ibexian (James et al., 1989).

A second TR sequence (TR-2) is present in the western part of the study area, but its top is truncated progressively updip and along strike toward the Beauge arch by the super-Romaine unconformity (Figure 4). The TR-2 is up to 10 m (33 ft) thick in the western Mingan Islands and passes basinward into 60 m (200 ft) of fossiliferous open-shelf muddy limestones beneath the northwestern part of Anticosti Island. The TR-2 records rapid deepening from peritidal conditions to open-marine conditions. The TR-2 is likely coeval with the demise of the great American carbonate bank at the St. Lawrence promontory (western Newfoundland) and is most likely coeval with the subaerial exposure and erosion of the upper part of the St. George Group (Aguathuna Formation) at the St. George unconformity and with super-unconformity strata that includes the basal part of the foreland shelf facies of the Table Point Formation, Table Head Group (James et al., 1989). The TR-2 would likely correlate in time and facies with the Carillon Formation in the adjacent inner part of the Quebec reentrant (Dix and Al Rodhan, 2006; Salad Hersi et al., 2007). Tectonics clearly was a key factor in the development of the sedimentary architecture during the early Whiterockian.

HYDROCARBON RESERVOIR POTENTIAL OF THE ROMAINE FORMATION

In eastern North America, Lower to Upper Ordovician carbonates are major oil and gas reservoirs (Hurley and Budros, 1990; Carter et al., 1996; Smith, 2006). Oil reservoirs have been found and described in Lower Ordovician strata of western Newfoundland (Garden Hill field; Cooper et al., 2001) and natural gas was produced until recently from Lower Ordovician dolomites of the St. Flavien field in southern Quebec (Bertrand et al., 2003). All of these Ordovician reservoirs are in dolostones whose origin has been ascribed to the circulation of late-stage hydrothermal fluids that increase the porosity by dissolution, allowing reservoirs to accumulate hydrocarbons and maintain petrophysical properties favorable to exploitation.

The hydrothermal dolomite model has been proposed for the Romaine Formation of the Anticosti Basin (Lavoie et al., 2005; Lavoie and Chi, 2010). Therefore, from western Newfoundland to the Appalachian Basin in the eastern United States, hydrothermal alteration of Lower Ordovician successions has generated significant fault-controlled regional masses of dolomites. The following section will summarize the petrographic and geochemical evidence supporting the pervasive dolomitization of both the intertidal and subtidal facies of the Romaine Formation by the circulation of exotic, high-temperature, and saline brines.

DIAGENESIS OF THE ROMAINE FORMATION

Petrographic study, using transmitted-light and cathodoluminescence microscopy, resulted in the recognition of early and late calcite diagenetic cementation

Figure 5. (A) A field photograph (cross section view) of laminated dolomicrite or dololaminite (lithofacies D) illustrating wavy to planar laminae and capping a peritidal cycle. Note the presence of mud cracks, which disrupt the laminae at their top. Île du Havre northwest, central Mingan Islands. (B) A polished slab (cross section view) of lithofacies E showing ripple-laminated interbeds (dark area) and structureless dolomicrite interbeds (light area). Note the soft-sediment deformation en echelon at the base of some laminated interbeds. Île du Havre northwest, central Mingan Islands. (C) A field photograph (bedding plane view) of closely spaced or laterally linked hemispheroid stromatolites (lithofacies F). Île du Havre west, central Mingan Islands. (D) A polished slab (vertical view) of lithofacies G with abundant gastropods from the base of the unit. Grande Île north, western Mingan Islands. (E) A field photograph (cross section view) of an ooid dolostone unit (lithofacies H) with small-scale cross-bedding. Île du Havre west, central Mingan Islands. (F) A field photograph showing the dendritic burrow-mottled network in relief (lithofacies B) and the more recessively weathered matrix (bedding plane view). Île à la Chasse east, eastern Mingan Islands. Lens cap is 50 mm in diameter. (G) A field photograph (bedding plane view) of thrombolite mound and adjacent flanking bed (lithofacies C). Mound is composed of coalescent meter-size thrombolites heads (h) exhibiting a macroscopic clotted appearance characterized by a cerebroidal pattern. Île à la Chasse northwest, eastern Mingan Islands. (H) A field photograph (cross section view) of an isolated thrombolite head (h) and flanking burrow-mottled dolostone (b). Baie Puffin E., eastern Mingan Islands. Hammer is 30 cm (12 in.).

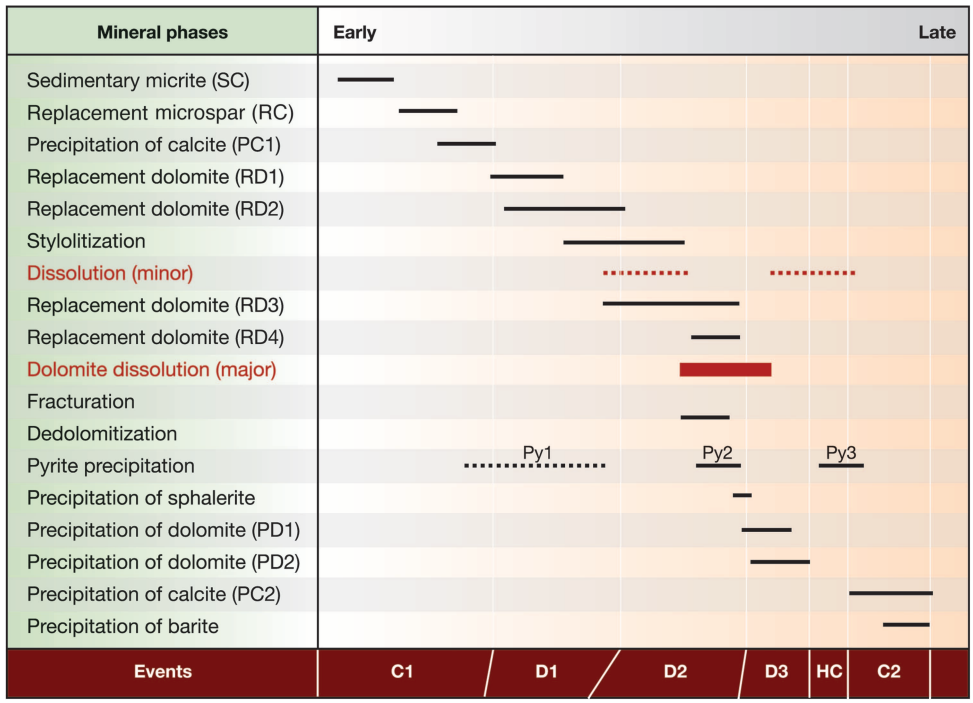

Figure 6. Summary of the paragenetic succession in the Romaine Formation as recognized from detailed conventional and cathodoluminescence petrography. Dotted lines represent uncertain time relationships. HC = main event of hydrocarbon migration; C = calcite diagenetic cementation; D = dolomitization. See text for details.

phases (C1 and C2) and three dolomitization events (D1 to D3) in the Romaine Formation (Brennan-Alpert, 2001; Lavoie et al., 2005) (Figure 6). Other significant diagenetic features (stylolites, sulfides, barite) and events (brecciation, dissolution) were also recognized. Fluid inclusions were studied for all carbonate phases (see Lavoie et al., 2005, and Lavoie and Chi, 2010, for detailed microthermometric results). More than 100 carbon and oxygen stable isotope and 11 strontium radiogenic isotope analyses were performed on these carbonate phases (Brennan-Alpert, 2001; Lavoie et al., 2005; Lavoie and Chi, 2010). At the regional scale, dolomitization of the Romaine Formation decreases basinward (southwesterly). Peritidal facies are pervasively dolomitized (D1–D3 events) everywhere, whereas subtidal facies are either pervasively dolomitized (Mingan Islands and onshore outcrops; D1–D3 events) or only partly dolomitized (Anticosti cores; D2 and D3 events).

Early Calcite Diagenesis (C1) Event

Fine-grained limestone, mainly composed of sedimentary micrite (SC) that is iron (Fe) poor, yellow luminescent under cathodoluminescence microscopy, and devoid of visible intercrystalline porosity, is replaced by microspar (RC). The latter is anhedral, 0.005 to 0.3 mm, Fe poor, and dully luminescent, and replaces both micrite and fossils. An early phase of pore-filling calcite (PC1) is anhedral, 0.1 to 0.5 mm, Fe poor, and characterized by zoned yellow/dull luminescence (Figure 3A). These three sedimentary and diagenetic phases represent C1 events. Fluid inclusion and geochemical data suggest that the C1 phases were either precipitated in the sedimentary environment (SC) or formed in near-surface diagenetic environments (RC and PC1). The three early calcite phases (C1 event) occur mainly in limestones that have not been subject to dolomitization.

First Dolomitization (D1) Event

The earliest dolomitization (D1) event is represented by two types of petrographically similar dolomite crystals. The first replacement dolomite (RD1) is anhedral to subhedral, mainly nonplanar, very fine grained (0.005–0.03 mm), and Fe rich, and shows dull reddish orange luminescence. The second phase of replacement dolomite (RD2) is similar to RD1, except that it is more coarsely crystalline (0.02–0.12 mm) and contains less Fe. The RD1 and RD2 can form interstratified parallel laminations that display sedimentary bedding and primary facies. These two phases of dolomite are the main components of the Romaine dolostones. They postdate C1 calcite and predate significant chemical compaction and stylolitization.

In general, RD1 is primarily found in peritidal depositional facies, whereas RD2 is more common in the subtidal facies assemblage. They do not possess intercrystalline porosity, but were locally subjected to later

dissolution that produced pore space in the Romaine Formation carbonates. Fluid inclusion results combined with geochemical data indicate that some recrystallization of a marine or very-shallow-burial dolomite precursor occurred in the presence of a relatively higher temperature, highly saline fluid (homogenization temperature [T_h] values of 55–98°C, average of 75°C, 20.4–24.2 wt. % NaCl equivalent). A few RD1 and RD2 samples are clearly depleted in ^{13}C with respect to marine carbonates. This suggests that some of the recrystallization occurred in the presence of significantly ^{13}C-depleted diagenetic fluids and could indicate the presence of a large volume of biogenic HCO_3^- that could be derived from thermochemical sulfate reduction of organic matter (Machel, 1987). The $^{87}Sr/^{86}Sr$ ratios that range between 0.709142 and 0.712862 (six analyses; Lavoie and Chi, 2010) compare with Lower Ordovician normal marine values (0.708750; Shields et al., 2003). These early dolomites are enriched in radiogenic strontium isotopes and suggest major interactions of the diagenetic fluids with rubidium (Rb)-rich phases that were likely derived from input of clastic sediments or from the Precambrian basement. The high-salinity values of the fluid inclusions (see above) and the oxygen isotopic composition ($\delta^{18}O_{SMOW}$) of the diagenetic fluid, based on paired T_h and $\delta^{18}O_{PDB}$ values of D1 phases, suggest that these radiogenic values could not be derived from meteoric waters. However, the diagenetic fluid had oxygen isotopic ratios of −4 to −2‰, which is consistent with a shallow-burial mix of seawater and burial brine (Lavoie and Chi, 2010). Nevertheless, the D1 dolomites appear to have been controlled by sedimentary textures, as indicated by their bedding-parallel distribution and apparently postdate the early calcites but predate other minerals. They were probably formed early in the diagenetic history of the Romaine Formation, before significant chemical compaction and stylolite formation (Figure 6). However, some RD2 dolomite may have been formed later and overlapped in time with later dolomite phases.

Second Dolomitization (D2) Event

This event is composed of two phases of dolomite (RD3 and RD4) replacement. These dolomites postdate compaction and are relatively unaffected by stylolitization, unlike RD1 and RD2 dolomites (Figure 6). The RD3 dolomite, in the third phase of replacement dolomite, is anhedral to euhedral, planar to nonplanar, 0.02 to 0.5 mm in crystal size, and Fe poor with or without a Fe-rich rim, and shows dull reddish orange luminescence with or without a bright reddish orange rim. The fourth replacement dolomite (RD4) is similar to dolomite RD3, except that it is uniformly Fe rich. In most cases, these two replacement dolomite phases are associated with fractures that contribute to significant secondary porosity. In addition, they both have abundant intercrystalline pore spaces and line inner surfaces of dissolution pores in RD1 and RD2 dolomites. The brightly luminescent rims of RD3 dolomite crystals are locally dissolved, suggesting more dissolution after the formation of RD3 dolomite. Fluid inclusions and stable isotopes of the D2 elements suggest that they were formed at higher temperatures (T_h values of 59–139°C, average of 99°C) than the D1 phases and were associated with wide ranging, but still highly saline fluid (12–26.6 wt. % NaCl equivalent). The D2 dolomite is associated with a fracture dissolution event that created porosity in D1 dolostone. Later, interstitial fluids were responsible locally for dedolomitization of some D2 dolomite rhombs (RD3 and RD4 dolomites). In places, RD3 dolomite shows a transitional relationship with RD2 dolomite, the main difference being that RD3 dolomite has more intercrystalline porosity. The $^{87}Sr/^{86}Sr$ ratios range between 0.709274 and 0.710208 (three analyses; Lavoie and Chi, 2010). Compared with Lower Ordovician normal marine values (0.708750; Shields et al., 2003), these dolomites are enriched in radiogenic strontium isotopes. The strontium isotope ratios suggest significant interactions between the diagenetic fluids and Rb-rich phases. As for the previous D1 phases, these radiogenic values could not be derived from meteoric waters as indicated by the high salinity of the fluid inclusions (see above). The calculation of the oxygen isotopic composition ($\delta^{18}O_{SMOW}$) of the diagenetic fluid based on paired T_h and $\delta^{18}O_{PDB}$ values of D2 phases suggests that the diagenetic fluid had oxygen isotopic ratios between +2 and +6‰, which is consistent with burial brines (Lavoie and Chi, 2010).

Third Dolomitization (D3) Event

Two types of vuggy pore- and fracture-filling dolomite cement (PD1 and PD2) are distinguished. The PD1 dolomite is subhedral to euhedral, planar to saddle, 0.1 to 0.5 mm in crystal size, Fe poor, and very dully reddish orange luminescent, and partly fills or lines vugs. The PD2 dolomite is similar to the PD1 dolomite, except that it is Fe rich and may have brighter reddish orange luminescent laminae. The PD2 dolomite may fill fractures and dissolution vugs. In some cores (drill cores 4 and 6 in Figure 1) significant collapse brecciation forms decimeter- to meter-thick intervals of dolomitic breccia that precede the precipitation of the void-filling dolomites. The two pore-filling dolomites (PD1 and PD2) do not coexist in the same pores or fractures but are similar in paragenetic position and are thus grouped as D3. Bitumen coating is observed on D3 crystal faces

(Figure 6). Fluid inclusion results and geochemical data indicate that a large part of D3 pore- and fracture-filling dolomite precipitated out of a high temperature (T_h values of 60–151°C, average of 111°C) and highly saline (17.0–26.5 wt. % NaCl equivalent) fluid. The D3 dolomite (PD1 and PD2) event postdates the brecciation-dissolution event and may partly overlap with D2 in time. The $^{87}Sr/^{86}Sr$ ratios of 0.709577 and 0.710594 were obtained (Lavoie and Chi, 2010) and are enriched in radiogenic strontium isotopes compared with Lower Ordovician normal marine values (0.708750; Shields et al., 2003). The strontium isotope ratios suggest significant interactions between the diagenetic fluids and Rb-rich phases. As with the previous D1 to D2 phases, these radiogenic values could not be derived from meteoric waters as indicated by the high salinity values of the fluid inclusions. The calculation of the oxygen isotopic composition ($\delta^{18}O_{SMOW}$) of the diagenetic fluid based on paired T_h and $\delta^{18}O_{PDB}$ values of D3 phases suggests that the diagenetic fluid had oxygen isotopic ratios between +2 and +3‰, which is consistent with burial brines (Lavoie and Chi, 2010). The coating of bitumen locally on D3 dolomite crystal faces indicates an influx of hydrocarbons in the post-D3-event diagenetic fluids.

Base Metal Precipitation

Sphalerite occurs as anhedral, coarse (1–8 mm), yellow to brown crystals that fill fractures or vugs in association with D3 dolomites. Sphalerite predates and locally partly overlaps the D3 event (Figure 6). Pyrite occurs either as fine crystals (0.5–2 mm) disseminated in replacement dolomites or as coarse crystals (2–10 mm) coating fractures and pores. Pyrite appears at multiple stages in the paragenetic succession (Figure 6), either associated with early calcite and D1 events or in later dissolution vugs lined by D2 to D3 dolomite or later calcite (PC2).

Late Calcite (C2) and Barite Precipitation

Late-phase pore-filling calcite (C2) is composed of anhedral crystals, 0.05 to 6 mm in size, that are Fe poor to Fe rich, fill fractures or vuggy pores still open after dolomite precipitation, and show yellowish orange luminescence with or without patches or irregular zones of dull luminescence. Barite cement fills fractures or vuggy pores and is associated with calcite C2 phase. Geochemical values indicate that the conditions were cooler during precipitation of the late calcite than the previous D3 phases, assuming a common fluid. This is also supported by the lower T_h values recorded by fluid inclusions in the C2 calcites (34–121°C, average of 79°C) and post-C2-event barite cements (51.5–110.6°C, average of 78°C). The C2 and barite fluid inclusions are also characterized by high salinity values (average of 23.3 and 23.4 wt. % NaCl equivalent, respectively), which support the interpretation of a common fluid for precipitation of D3 dolomite and C2 calcite and barite cements. Some late calcites commonly host hydrocarbon fluid inclusions (Lavoie et al., 2005), supporting the presence of hydrocarbons in the late diagenetic fluid system. Both C2 calcite and barite occupy a similar paragenetic position (Figure 6) in that they both postdate the dissolution-brecciation event as well as the D3 dolomite and bitumen. In the early phases of the Taconic foreland basin (Lavoie and Chi, 2010), hot brines circulated in the Grenvillian basement where they got their Mg^{2+} charge (Lavoie et al., 2010). The hydrothermal fluid migrated upward along active foreland faults, resulting in the D2 and D3 events recorded in the Romaine carbonates and breccia (Lavoie et al., 2005). The high-temperature brine was responsible for leaching of precursor carbonates and local massive dolomitization in both the Romaine and overlying Mingan carbonates (Lavoie and Chi, 2010) (Figure 7). Most of the tectonic movements along ancestral rift-related and newly formed foreland faults ceased after the rapid deepening that led to the sedimentation of mostly undiluted siliciclastic muds of the Upper Ordovician Macasty Formation that sealed off the foreland faults (Lavoie et al., 2005; Lavoie and Chi, 2010). The rapid and efficient extensional-fault-driven migration of Mg^{2+}-rich high-temperature brine was then mostly stopped, and the Mg-poor slowly cooling brines were responsible for the deep burial precipitation of C2 and the small volume of barite in local voids and fractures.

Dedolomitization

Partial to sometimes complete and extensive dedolomitization (calcitization of dolomite of the D2 event, Figure 6) is observed in the northern and eastern wells of Anticosti Island (Brennan-Alpert, 2001; Lynch and Trollope, 2001).

EXPLORATION PLAY TYPES OF THE WESTERN ANTICOSTI BASIN

The Ordovician–Silurian strata on Anticosti Island form a southwesterly dipping homoclinal succession without significant folds. Various play concepts were tested beneath Anticosti Island, including diagenetic closure along the super-Romaine unconformity or structural closure along synsedimentary faults, but these plays

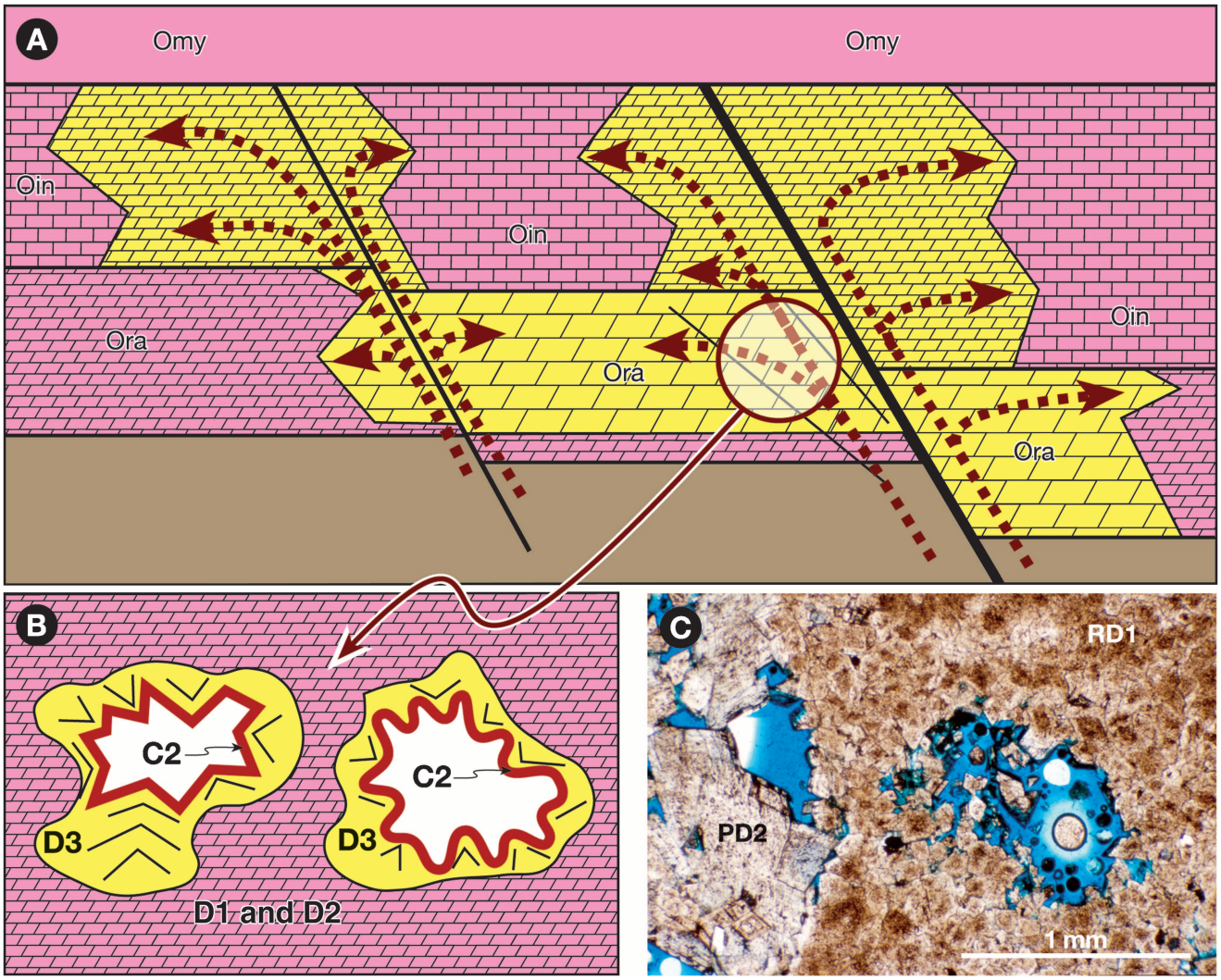

Figure 7. (A) Hydrothermal dolomitization model for the Anticosti carbonates. Hydrothermal fluids used extensional foreland faults to migrate upward. Lateral fluid movement occurred at impermeable barriers such as the Romaine (Ora) top unconformity or at the contact between the Mingan Limestone (Oin) and Macasty Shale (Omy). See text for details. Not to scale. (B) Schematic close-up of secondary pore spaces in the dolomites of the Romaine Formation (Ora). The Romaine background consists of D1 and D2 replacement dolomites. The dissolution voids are filled by D3 pore-filling dolomite cements. The saddle dolomite crystals in D3 are locally coated by C2 pore-filling calcite cements or bitumen. (C) Photomicrograph of blue epoxy impregnated dolomite of the Romaine Formation. The background consists of the small crystals RD1 of the D1 event. The D1 matrix dolomite is locally dissolved, with resulting pore space partly filled by large saddle dolomite crystals PD2 of the D3 event. Open pore space in blue.

produced meager exploration results (Lynch, 2001). Petrographic and geochemical attributes, combined with the other geologic and geophysical evidence, however, support the interpretation that the Lower Ordovician carbonates of Anticosti Island were hydrothermally altered and formed porous structurally controlled dolostone reservoirs (Lavoie et al., 2005; Lavoie and Chi, 2010) (Figure 7).

Saddle dolomite is ubiquitous in the Lower Ordovician Romaine Formation, either as vug- and fracture-filling cement or as a replacement of previous carbonate. It is intimately associated with minor sphalerite (Mississippi Valley-type) mineralization and commonly succeeded by late calcite-sulfate cements (Lavoie and Chi, 2010). Bitumen locally postdates the saddle dolomite. Migration of high-temperature diagenetic fluids commonly leads to dissolution and corrosion of the precursor host rock, localized to pervasive dolomitization, and an almost universal paragenetic suite of base metal sulfides, saddle dolomite, with or without bitumen,

calcite, and calcium sulfate (Davies and Smith, 2006). The saddle dolomites of the Romaine Formation (PD1 and PD2) show a typical hydrothermal signature with high homogenization temperatures and high-salinity fluid inclusions. This is particularly significant for wells and outcrops near the northern erosional edge of the basin, where paleoburial depth and temperatures were independently shown to be lower than that of fluid inclusions in the D3 saddle dolomite (Bertrand, 1987, 1990).

Thicker sedimentary successions on the seismic profiles (Roksandic and Granger, 1981; Lynch and Trollope, 2001; Castonguay et al., 2005) occur on the downthrown blocks of extensional faults (Figure 2B). These faults were episodically active from the late Ibexian (Romaine) until the end of the Caradocian (lower part of the Vaureal), a time interval roughly coincident with the main phase of Taconic accretion at the outboard margin of Laurentia (Van Staal et al., 1998). In addition, seismic data across Anticosti Island clearly show fault-bounded collapsed segments or sags from the Romaine Formation to the top of the Mingan Formation as well as significant loss of seismic marker continuity (Lynch and Trollope, 2001).

The porous, structurally controlled hydrothermal dolomite facies in the Romaine Formation provide an attractive trapping mechanism for migrating hydrocarbons along the southwesterly dipping Anticosti homoclinal succession. Lateral and vertical diagenetic seals of these porous dolostone reservoirs are formed by the encasing tight nonporous dolostone-limestone succession (Figure 7). The secondary porosity generated during hydrothermal dolomitization subsequently allowed hydrocarbon migration as suggested by their presence as inclusions in the late calcite precipitates. The hydrocarbons were derived from the organic carbon-rich Macasty Formation (total organic carbon up to 6%; Bertrand, 1987), which lies above the Mingan Formation. It has been assumed from previous exploration activities that hydrocarbon migration occurred through normal updip pathways from structurally lower, but stratigraphically higher, beds resulting from the local tectonic juxtaposition of downthrown Middle Ordovician source rocks below upthrown Lower Ordovician dolomite reservoirs (Figure 7). The latter extensional fault-controlled scenario has been recognized on many seismic lines and has served as an exploration guide in the recent round of exploration on the Anticosti Island (Lynch, 2001). However, recent thermal and pressure modeling (Chi et al., 2010) suggests that some downward hydrocarbon migration is possible from the local development of overpressures in the Macasty Formation. The exact timing of primary hydrocarbon migration is unknown but has long been equivocally suggested to have occurred during or after the Early Devonian (Bertrand, 1990). However, the recent modeling exercise suggests that initial oil generation could have occurred in the late Early Silurian (Chi et al., 2010). The occurrence of oil inclusions in late-formed calcite cement and barite indicates petroleum migration after the formation of dolomitization-related porosity.

CONCLUSIONS

1) Lower Ordovician to lower Middle Ordovician (upper Ibexian to lower Whiterockian; upper Sauk III supersequence) carbonates of the Romaine Formation in the western Anticosti Basin record the evolution of the early Paleozoic low-latitude passive margin of eastern North America. The carbonates are bound by a basal unconformity on Precambrian basement and by a capping unconformity, the super-Romaine unconformity that separates the Romaine from the overlying Mingan Formation and marks the Sauk-Tippecanoe boundary in the study area. Local and regional stratigraphic relationships within these passive-margin carbonates, however, suggest that significant tectonic activity, related to the earliest phases of a developing Taconic foreland basin, encroached on the platform succession, before subaerial exposure and final demise of the Lower Ordovician great American carbonate bank occurred in the Whiterockian (super-Romaine unconformity).
2) The Romaine Formation is mostly composed of peritidal and open-shelf carbonates deposited during two large-scale third-order TR sequences that are correlated basinward into the subsurface beneath the Anticosti Island. The first of these sequences followed initial flooding of Precambrian basement in the late Ibexian. Localized peritidal deposition was quickly supplanted, as sea level rose across the Romaine platform, leading to dominantly open subtidal deposition. The latter includes the transition from transgressive systems tract to RST deposition, including mound-dominated deposition as the platform gave way to regional peritidal deposition. The peritidal rocks also include the sequence boundary to the second sequence, which comprises open subtidal deposition at the topmost interval of the preserved Romaine section during the early Whiterockian. Regional erosional and karsting truncates the two sequences at the super-Romaine unconformity.
3) Petrographic, fluid inclusion, and isotope data indicate that the dolostones of the Romaine Formation formed from early diagenetic to late-stage

hydrothermal dolomization. Early diagenetic dolomitization (D1 event), which is essentially synsedimentary to early shallow burial, did not create porosity. Significant porosity, however, was produced during the D2 and D3 dolomitization events that were associated with high-temperature highly saline fluids. This, combined with other geologic and geophysical data, provides evidence that the Lower Ordovician carbonates were hydrothermally altered to form porous structurally controlled dolostone reservoirs.

ACKNOWLEDGMENTS

This chapter benefited from the initial review of Keith Dewing and from the detailed and critical reviews of Ian Knight and Bill Morgan. We thank Shell Canada, Encal Energy, Hydro-Quebec (former Oil and Gas Division), and Corridor Resources for significant support at various stages of this research. The Natural Sciences and Engineering Research Council of Canada, the Natural Resources of Canada National Geoscience Mapping (NATMAP) Program, the Targeted Geoscience Initiative Program, and the Ontario Government Science and Technology Scholarship program all provided research support. The Ministère des Ressources Naturelles et de la Faune du Quebec allowed access to cores from the Anticosti Island. This is Geological Survey of Canada Contribution 20080361.

REFERENCES CITED

Bertrand, R., 1987, Maturation thermique et potentiel pétroligène des series post-taconiennes du nord-est de la Gaspésie et de l'île d'Anticosti: Thèse de doctorat, Université de Neuchâtel, Neuchâtel, Switzerland, 647 p.

Bertrand, R., 1990, Maturation thermique et histoire de l'enfouissement et de la génération des hydrocarbures du bassin de l'archipel de Mingan et de l'Île d'Anticosti: Canadian Journal of Earth Sciences, v. 27, p. 731–741, doi:10.1139/e90-075.

Bertrand, R., A. Chagnon, Y. Duchaine, D. Lavoie, M. Malo, and M. M. Savard, 2003, Sedimentologic, diagenetic, and tectonic evolution of the Saint-Flavien gas reservoir at the structural front of the Quebec Appalachians: Bulletin of Canadian Petroleum Geology, v. 51, p. 126–154, doi:10.2113/51.2.126.

Bordet, E., M. Malo, and D. Kirkwood, 2010, Structural study of western Anticosti Island, St. Lawrence platform, Quebec: Fracture analysis and integration of surface and subsurface structural data: Bulletin of Canadian Petroleum Geology, v. 58, p. 36–55, doi:10.2113/gscpgbull.58.1.36.

Brennan-Alpert, P., 2001, Regional deposition and diagenesis of Lower Ordovician epeiric, platform carbonates: The Romaine Formation, Mingan Archipelago and subsurface Anticosti Island, eastern Quebec: M.Sc. thesis, University of Ottawa, Ottawa, Ontario, Canada, 107 p.

Carter, T., R. Trevail, and R. Easton, 1996, Basement controls on some hydrocarbon traps in southern Ontario, Canada, *in* B. A. Van der Pluijm and P. A. Catacosinos, eds., Basement and basins of eastern North America: Geological Society of America Special Paper 308, p. 95–107.

Castonguay, S., R. A. Wilson, D. Brisebois, A. Desrochers, and M. Malo, 2005, Compilation géologique, Anticosti-Gaspé-Campbellton, Les ponts géologiques de l'est du Canada, Transect 4, Québec-Nouveau-Brunswick: Geological Survey of Canada Open-File Report 4883, 1/125,000, 4 sheets.

Chi, G., and D. Lavoie, 2001, A diagenetic study of dolostones of the Lower Ordovician Romaine Formation, Anticosti Island, Quebec: Current research: Geological Survey of Canada, v. 2001-D17, 13 p.

Chi, G., D. Lavoie, R. Bertrand, and M.-K. Lee, 2010, Downward hydrocarbon migration predicted from numerical modeling of fluid overpressure in the Paleozoic Anticosti Basin, eastern Canada: Geofluids, v. 10, p. 334–350, doi:10.1111/j.1468-8123.2010.00280.x.

Cooper, M., J. Weissenberger, I. Knight, D. Hostad, D. Gillespie, H. Williams, E. Burden, J. Porter-Chaudhry, D. Ray, and E. Clark, 2001, Basin evolution in western Newfoundland: New insights from hydrocarbon exploration: AAPG Bulletin, v. 85, p. 393–418.

Davies, G. R., and L. B. Smith, 2006, Structurally controlled hydrothermal dolomite facies: An overview: AAPG Bulletin, v. 90, p. 1641–1690, doi:10.1306/05220605164.

Demicco, R. V., and L. A. Hardie, 1994, Sedimentary structures and early diagenetic features of shallow-marine carbonate deposits: SEPM Atlas Series 1, 265 p.

Desrochers, A., 1985, The Lower and Middle Ordovician platform carbonates of the Mingan Islands, Quebec: Stratigraphy, sedimentology, paleokarst, and limestone diagenesis: Ph.D. thesis, Memorial University of Newfoundland, St. John's, Newfoundland, Canada, 454 p.

Desrochers, A., and É. L. Gauthier, 2009, Carte géologique de l'île d'Anticosti: Ministère des Ressources naturelles et de la Faune du Québec, DV 2009-03, scale 1:250,000, 1 sheet.

Desrochers, A., and N. P. James, 1988, Early Paleozoic surface and subsurface paleokarst: Middle Ordovician carbonates, Mingan Islands, Quebec, *in* N. P. James and P. W. Choquette, eds., Paleokarst: New York, Springer-Verlag, p. 183–210.

Dix, G. R., 2012, The Sauk-Tippecanoe megasequence boundary in an interior structural corridor (Ottawa embayment) of the great American carbonate bank, *in* J. R. Derby, R. D. Fritz, S. A. Longacre, W. A. Morgan, and C. A. Sternbach, eds., The great American carbonate bank: The geology and economic resources of the Cambrian–Ordovician Sauk megasequence of Laurentia: AAPG Memoir 98, p. 545–557.

Dix, G. R., and Z. Al Rodhan, 2006, A new Middle Ordovician

geological framework for the Middle Ordovician Carillon Formation (uppermost Beekmantown Group, Ottawa embayment): Onset of Taconic foreland deposition and tectonism in the Laurentian platform interior: Canadian Journal of Earth Sciences, v. 43, p. 1367–1387, doi:10.1139/e06-030.

Hurley, N. F., and R. Budros, 1990, Albion-Scipio and Stoney Point fields, U.S.A., Michigan Basin, *in* E. A. Beaumont and N. H. Foster, eds., Stratigraphic traps 1: AAPG Treatise of Petroleum Geology, Atlas of Oil and Gas Fields, p. 1–38.

James, N. P., 1981, Megablocks of calcified algae in the Cow Head Breccia, western Newfoundland: Vestiges of a Cambro–Ordovician platform margin: Geological Society of America Bulletin, v. 92, p. 799–811, doi:10.1130/0016-7606(1981)92<799:MOCAIT>2.0.CO;2.

James, N. P., R. K. Stevens, C. R. Barnes, and I. Knight, 1989, Evolution of a lower Paleozoic continental-margin carbonate platform, northern Canadian Appalachians, *in* P. D. Crevello, J. L. Wilson, J. F. Sarg, and J. F. Read, eds., Controls on carbonate platform and basin development: SEPM Special Publication 44, p. 123–146.

Knight, I., and N. P. James, 1987, Stratigraphy of the Lower Ordovician St. George Group, western Newfoundland: The interaction between eustasy and tectonics: Canadian Journal of Earth Sciences, v. 24, p. 1927–1951, doi:10.1139/e87-185.

Knight, I., N. P. James, and T. E. Lane, 1991, The Ordovician St. George unconformity, northern Appalachians: The relationship of plate convergence at the St. Lawrence promontory to the Sauk-Tippecanoe sequence boundary: Geological Society of America Bulletin, v. 103, p. 1200–1225, doi:10.1130/0016-7606(1991)103<1200:TOSGUN>2.3.CO;2.

Lavoie, D., 1994, Diachronous tectonic collapse of the Ordovician continental margin, eastern Canada: Comparison between the Quebec reentrant and the St. Lawrence promontory: Canadian Journal of Earth Sciences, v. 31, p. 1309–1319, doi:10.1139/e94-113.

Lavoie, D., 2008, Appalachian foreland basin of Canada, *in* A. D. Miall, ed., Sedimentary basins of the world: The sedimentary basins of the United States and Canada: Amsterdam, Elsevier Science, v. 5, p. 65–103.

Lavoie, D., and G. Chi, 2010, Lower Paleozoic foreland basins in eastern Canada: Tectonothermal events recorded by faults, fluids and hydrothermal dolomites: Bulletin of Canadian Petroleum Geology, v. 58, p. 17–35.

Lavoie, D., E. Burden, and D. Lebel, 2003, Stratigraphic framework for the Cambrian–Ordovician rift and passive-margin successions from southern Quebec to western Newfoundland: Canadian Journal of Earth Sciences, v. 40, p. 177–205, doi:10.1139/e02-078.

Lavoie, D., G. Chi, P. Brennan-Alpert, A. Desrochers, and R. Bertrand, 2005, Hydrothermal dolomitization in the Lower Ordovician Romaine Formation of the Anticosti Basin: Significance for hydrocarbon exploration: Bulletin of Canadian Petroleum Geology, v. 53, p. 454–472, doi:10.2113/53.4.454.

Lavoie, D., S. Jackson, and I. Girard, 2010, Mg isotopes and hydrothermal saddle dolomites: Current data for Paleozoic dolomites of eastern Canada and implications for Mg source (abs.): Calgary, GeoCanada, Program with Abstracts.

Long, D. G. F., 2007, Tempestite frequency curves: A key to Late Ordovician and Early Silurian subsidence, sea level change and orbital forcing in the Anticosti foreland basin, Quebec, Canada: Canadian Journal of Earth Sciences, v. 44, p. 413–431, doi:10.1139/e06-099.

Lynch, G., 2001, Shell Canada-ENCAL Energy, Anticosti Island exploration 1997–2000: Shell Canada Limited, Annual Report, 2000TD456-01.

Lynch, G., and S. W. Trollope, 2001, Dolomitization, platform collapse, and reservoir development in Ordovician carbonates of Anticosti Island, Gulf of St. Lawrence: Canadian Society of Petroleum Geologists Annual Meeting Program with Abstracts, p. 126-1–126-6.

Machel, H. G., 1987, Saddle dolomite as a by-product of chemical compaction and thermochemical sulfate reduction: Geology, v. 15, p. 936–940, doi:10.1130/0091-7613(1987)15<936:SDAABO>2.0.CO;2.

Mossop, G. D., K. E. Wallace-Dudley, G. G. Smith, and J. C. Harrison, 2004, Sedimentary basins of Canada: Geological Survey of Canada Open-File Report 4673, scale 1: 5,000,000, 1 sheet.

Pinet, N., M. Duchesne, D. Lavoie, A. Bolduc, and B. Long, 2008, Surface and subsurface signatures of gas seepage in the St. Lawrence Estuary (Canada): Significance to hydrocarbon exploration: Marine and Petroleum Geology, v. 25, p. 271–288, doi:10.1016/j.marpetgeo.2007.07.011.

Pohler, S. M. L., C. R. Barnes, and N. P. James, 1987, Reconstructing a lost faunal realm; conodonts from the megaconglomerates of the Ordovician Cow Head Group, western Newfoundland, *in* R. L. Austin, ed., Conodonts: Investigative techniques and applications: Chichester, United Kingdom, Ellis Horwood, p. 341–362.

Pratt, B. R., and N. P. James, 1986, The St. George Group (lower Ordovician) of western Newfoundland: Tidal flat island model for carbonate sedimentation in epeiric seas: Sedimentology, v. 33, p. 313–343, doi:10.1111/j.1365-3091.1986.tb00540.x.

Roksandic, M. M., and B. Granger, 1981, Structural styles of Anticosti Island, Gaspé Passage, and eastern Gaspé Peninsula inferred from reflection seismic data, *in* P. J. Lespérance, ed., Anticosti-Gaspé: 2. Stratigraphy and paleontology: Université de Montréal, Montréal, Québec, Subcommission of Silurian Stratigraphy, Field Meeting of the Ordovician–Silurian Boundary Working Group, p. 211–221.

Salad Hersi, O., and G. R. Dix, 2006, Precambrian fault systems as control on regional differences in relative sea level along the Early Ordovician platform of eastern North America: Journal of Sedimentary Research, v. 76, p. 700–716, doi:10.2110/jsr.2006.016.

Salad Hersi, O., D. Lavoie, and G. S. Nowlan, 2003, Sedimentologic and biostratigraphic reappraisal of the Beekmantown Group of the Montreal area, southwestern Quebec:

Implications for the depositional evolution of the Lower–Middle Ordovician Laurentian margin of eastern Canada: Canadian Journal of Earth Sciences, v. 40, p. 149–176, doi:10.1139/e02-077.

Salad Hersi, O., G. S. Nowlan, and D. Lavoie, 2007, A revision of the stratigraphic nomenclature of the Cambrian–Ordovician strata of the Philipsburg tectonic slice, southern Quebec: Canadian Journal of Earth Sciences, v. 44, p. 1775–1790.

Sanford, B. V., 1993, St. Lawrence platform: Geology, *in* D. F. Stott and J. D. Aitken, eds., Sedimentary cover of the craton in Canada: Geological Survey of Canada, Geology of Canada, v. 5, p. 723–786.

Sanford, B. V., 1998, Geology and oil and gas possibilities of the Gulf of St. Lawrence region, southeast Canada: Geological Survey of Canada Open-File Report 3632, 39 p.

Shields, G. A., G. A. F. Carden, J. Veizer, T. Meidla, J.-Y. Rong, and R.-Y. Li, 2003, Sr, C, and O isotope geochemistry of Ordovician brachiopods: A major isotopic event around the Middle–Late Ordovician transition: Geochimica et Cosmochimica Acta, v. 67, p. 2005–2025, doi:10.1016/S0016-7037(02)01116-X.

Sloss, L. L., 1963, Sequences in the cratonic interior of North America: Geological Society of America Bulletin, v. 100, p. 1661–1665, doi:10.1130/0016-7606(1988)100<1661:FYOSS>2.3.CO;2.

Smith, L. B., 2006, Origin and reservoir characteristics of Upper Ordovician Trenton–Black River hydrothermal dolomite reservoirs in New York, U.S.A.: AAPG Bulletin, v. 90, p. 1691–1718, doi:10.1306/04260605078.

Thomas, W. A., 1977, Evolution of Appalachian-Ouachita salients and recesses from reentrants and promontories in the continental margin: American Journal of Science, v. 277, p. 1233–1278, doi:10.2475/ajs.277.10.1233.

Van Staal, C. R., J. F. Dewey, C. MacNiocaill, and W. S. McKerrow, 1998, The Cambrian–Silurian tectonic evolution of the northern Appalachians and British Caledonides: History of a complex, west and southwest Pacific-type segment of Iapetus, *in* D. J. Blundell and A. C. Scott, eds., Lyell: The past is the key to the present: Geological Society (London) Special Publication 143, p. 199–242.

Wilson, J. L., P. L. Medlock, R. D. Fritz, K. L. Canter, and R. G. Geesaman, 1992, A review of Cambro–Ordovician breccias in North America, *in* M. P. Candelaria and C. L. Reed, eds., Paleokarst, karst-related diagenesis, and reservoir development: SEPM-Permian Basin Section, Publication 92-33, p. 19–29.